Adiabatic Excitation for ^{31}P MR Spectroscopy in the Human Heart at 7 T: A Feasibility Study

Ladislav Valkovič,[1,2]* William T. Clarke,[1] Lucian A.B. Purvis,[1] Benoit Schaller,[1] Matthew D. Robson,[1] and Christopher T. Rodgers[1]

Purpose: Phosphorus magnetic resonance spectroscopy (^{31}P-MRS) provides a unique tool for assessing cardiac energy metabolism, often quantified using the phosphocreatine (PCr)/adenosine triphosphate (ATP) ratio. Surface coils are typically used for excitation for ^{31}P-MRS, but they create an inhomogeneous excitation field across the myocardium, producing undesirable, spatially varying partial saturation. Therefore, we implemented adiabatic excitation in a 3D chemical shift imaging (CSI) sequence for cardiac ^{31}P-MRS at 7 Tesla (T).

Methods: We optimized an adiabatic half passage pulse with bandwidth sufficient to excite PCr and γ-ATP together. In addition, the CSI sequence was modified to allow interleaved excitation of PCr and γ-ATP, then 2,3-DPG, to enable PCr/ATP determination with blood correction. Nine volunteers were scanned at 2 transmit voltages to confirm that measured PCr/ATP was independent of B_1^+ (i.e. over the adiabatic threshold). Six septal voxels were evaluated for each volunteer.

Results: Phantom experiments showed that adiabatic excitation can be reached at the depth of the heart using our pulse. The mean evaluated cardiac PCr/ATP ratio from all 9 volunteers corrected for blood signal was 2.14 ± 0.16. Comparing the two acquisitions with different voltages resulted in a minimal mean difference of -0.005.

Conclusion: Adiabatic excitation is possible in the human heart at 7 T, and gives consistent PCr/ATP ratios. **Magn Reson Med 78:1667–1673, 2017. © 2016 The Authors Magnetic Resonance in Medicine published by Wiley Periodicals, Inc. on behalf of International Society for Magnetic Resonance in Medicine. This is an open access article under the terms of the Creative Commons Attribution License, which permits use, distribution and reproduction in any medium, provided the original work is properly cited.**

Key words: high energy phosphate; ^{31}P-MRS; ^{31}P; heart; ultra-high field; 7T; 7 Tesla; adiabatic

INTRODUCTION

Phosphorus MR spectroscopy (^{31}P-MRS) allows noninvasive assessment of concentrations and/or reaction kinetics of high-energy metabolites such as adenosine triphosphate (ATP) and phosphocreatine (PCr) in vivo (1–5). ^{31}P-MRS is of particular interest in cardiovascular medicine (6), as the PCr/ATP ratio in the heart changes in most major heart diseases, e.g., myocardial infarction (7), failing hypertrophied myocardium (8), or dilated cardiomyopathy (9,10), where it can even serve as a predictor of mortality (11). The cardiac PCr/ATP ratio is also impaired in systemic diseases such as type 2 diabetes (12,13) and in obesity (14).

Still, cardiac ^{31}P-MRS is not yet recognized as a practical tool for clinical applications. This is primarily because of the inherently low signal-to-noise ratio (SNR) for ^{31}P-MRS on clinical MR systems operating at less than or equal to 3 Tesla (T). To overcome this restraint, ultra-high fields (e.g., 7 T), leading to more than doubled SNR (4,15–17) and/or increased temporal resolution (18), are being used ever more often for ^{31}P-MRS. Further improvement in SNR for cardiac ^{31}P-MRS, accompanied with enhanced heart coverage, was recently demonstrated using a dedicated receive array combined with a single-loop transmit radiofrequency (RF) coil at 7 T (19,20).

Although achieving excellent receive sensitivity, the transmit performance (B_1^+) of surface coils varies strongly depending on the exact position of the coil relative to the volume of interest, especially at ultra-high fields. Accurate knowledge of flip angle (FA) in a given voxel is essential for reliable correction of partial saturation, which is required to determine metabolite concentrations or ratios (21). Computing field maps using quasi-static approximation becomes increasingly inaccurate at ultra-high fields, and direct measurement of FA maps requires additional acquisition time (22–24). The use of B_1^+-insensitive adiabatic excitation providing uniform $90°$ excitation FAs over the whole heart, as demonstrated at lower fields (25,26), would therefore constitute a significant improvement for cardiac ^{31}P-MRS at 7 T and provide an important step toward absolute quantification. However, application of adiabatic excitation pulses at 7 T is

challenging because of their high B_1^+ requirements, high specific absorption rates (SARs), and because of the wide bandwidth (BW) of ^{31}P-MR spectra.

However, because the key metabolites of interest for cardiac ^{31}P-MRS are PCr and ATP, we hypothesized that a reduced excitation BW of the adiabatic half-passage (AHP) pulse could be traded to decrease the required B_1^+ and SAR, while still exciting over a frequency range from PCr to γ-ATP. This work benefits from the improved B_1^+ ($\geq 16\,\mu$T) at the "depth of the heart," i.e. at a distance of the intraventricular septum from the center of the coil (8–12 cm, depending on individual anatomy), provided by a purpose-built quadrature ^{31}P transceiver coil (27). Therefore, the aim of this study was to test the feasibility of a narrow-band ($\sim$300 Hz) adiabatic excitation for cardiac ^{31}P-MR 3D chemical shift imaging (CSI) at 7 T. In addition, to enable blood correction of the calculated PCr/ATP ratio, an interleaved acquisition of the 2,3-diphosphoglycerate (2,3-DPG) resonance frequency was implemented.

METHODS

Hardware

All measurements were performed on a 7T whole-body MR system (Siemens Healthcare, Erlangen, Germany) equipped with a dual-tuned (^{31}P/^{1}H) transmit-receive quadrature, surface RF coil, consisting of a purpose-built quadrature ^{31}P coil (two 15-cm loops, with overlap decoupling) and a single ^{1}H loop (10 cm in diameter). The peak B_1^+ of this coil across the heart was estimated to be between 16 and 25 μT (27).

Pulse Simulations and Sequence Design

A dedicated AHP excitation pulse (tanh/tan) (28) was adjusted using Bloch simulations through a manual tuning of its parameters (i.e. duration between 2.5 and 15 ms, ξ between 1 and 20, tan(κ) between 5 and 100 rad, and frequency sweep between 5 and 50 kHz). The main target was to obtain a low adiabatic threshold B_1^+ ($<$16 μT) and to minimize the SAR requirements, while maintaining a BW of at least 300 Hz at the depth of the heart. The resulting AHP pulse was 7.5 ms long, with its shape defined by $\xi = 3$ and tan(κ) $= 85$ rad and with a frequency sweep bandwidth of 25 kHz (Fig 1a). Bloch simulations of the excitation performance, e.g., magnetization in the xy plane (M_{xy}) and FA of the selected pulse were performed for B_1^+ values from 0 to 40 μT using custom MATLAB (Math-Works, Natick, MA) routines. Figures 1b and 1c depict the M_{xy} and the excitation FA distribution of the selected AHP pulse, respectively. The dependence of M_{xy} on transmit voltage, visualized in Figure 1d, demonstrates the stability of M_{xy} value above the adiabatic threshold at 7 μT. The simulated off-resonance excitation profile (i.e. BW) of the AHP pulse for the minimal B_1^+ expected at the "depth of heart" (16 μT) is depicted in Figure 1e.

Because of the narrowness of the designed AHP-pulse BW at 7 T, only PCr and γ-ATP resonance will be excited equally using this pulse. Although this is sufficient for straightforward PCr/ATP ratio evaluation, no information about the 2,3-DPG signals, originating from the blood pool and necessary to correct for the blood-ATP signal (29),

would be available. Therefore, an ultra-short echo time (UTE) 3D-CSI (30) pulse sequence was modified to allow multiple excitations in an interleaved scheme. The excitation frequency offset was first targeted between the PCr and γ-ATP resonances and then between the two peaks of 2,3-DPG. As the BW of the AHP pulse is also asymmetric (Fig. 1e), the excitation frequency of the first acquisition was not centered exactly between the PCr and γ-ATP signals, but instead was positioned closer to the γ-ATP resonance frequency (i.e. at -175 Hz relative to the PCr). The excitation and acquisition at the second frequency (centered between the two peaks of 2,3-DPG at 700 Hz) was performed in every other transient. As the off-resonance phase of the pulse is nonlinear on one side, two-step phase-cycling was used to avoid disrupting the metabolites of interest during the other excitation.

Phantom Experiments

The performance of the adjusted AHP pulse was tested using a two-compartment phantom (4), which consists of an 18 L chamber filled with saline, providing coil loading similar to that of a lean volunteer, and a $2 \times 2 \times 2$ cm^3 cube filled with a solution of KH$_2$PO$_4$ doped with Gd-DTPA (T$_1 = \sim$1.7 s). The cube was fixed at a depth of 8 cm, simulating the position of myocardium in vivo, and the RF coil was placed on top of the phantom. Fully relaxed (repetition time (TR) $= 10$ s), nonlocalized, single-average ^{31}P-MRS spectra were acquired on-resonance using the UTE-CSI sequence with the transmitter voltage increasing from 10 to 310 V in 50-V steps, and above in 20-V steps up to the maximum voltage of 470 V. The off-resonance behavior of the AHP pulse was tested by acquiring ^{31}P-MRS spectra using the same sequence at the maximum voltage, by shifting the central excitation frequency in 25-Hz steps from -300 to 300 Hz.

In Vivo Experiments

Nine healthy volunteers (two females; age [mean $\pm$ standard deviation] 28.2 $\pm$ 5.3 years; body mass index (BMI) 22.8 $\pm$ 2.6 kg.m^{-2}) were recruited and scanned in compliance with ethical and legal requirements. Subjects were measured in supine position, which was preferred over the prone position to maximize the volunteer comfort, even at the cost of increased breathing motion, with the RF coil positioned over their heart. The RF coil was tuned and matched before each examination to account for the potential differences in RF loading. Only small adjustments were needed between subjects, suggesting that coil loading and thus B_1^+ efficiency was similar for all subjects. CINE FLASH images were acquired using pulse oximeter gating (Siemens, München, Germany), and the UTE-CSI matrix was then aligned to the short-axis (SA) images. To test the adiabatic excitation in vivo, the cardiac 3D ^{31}P UTE-CSI scan using the interleaved excitation with the selected AHP pulse was repeated twice in each volunteer. First, at a transmit voltage giving 100% predicted SAR (i.e. $\sim$450 V) and then at 50 V less. This was also used to assess the scan-to-scan reproducibility. Because of SAR restrictions, relatively long TR (3000 ms) was mandatory between individual transients (the effective TR for each interleaved data set was
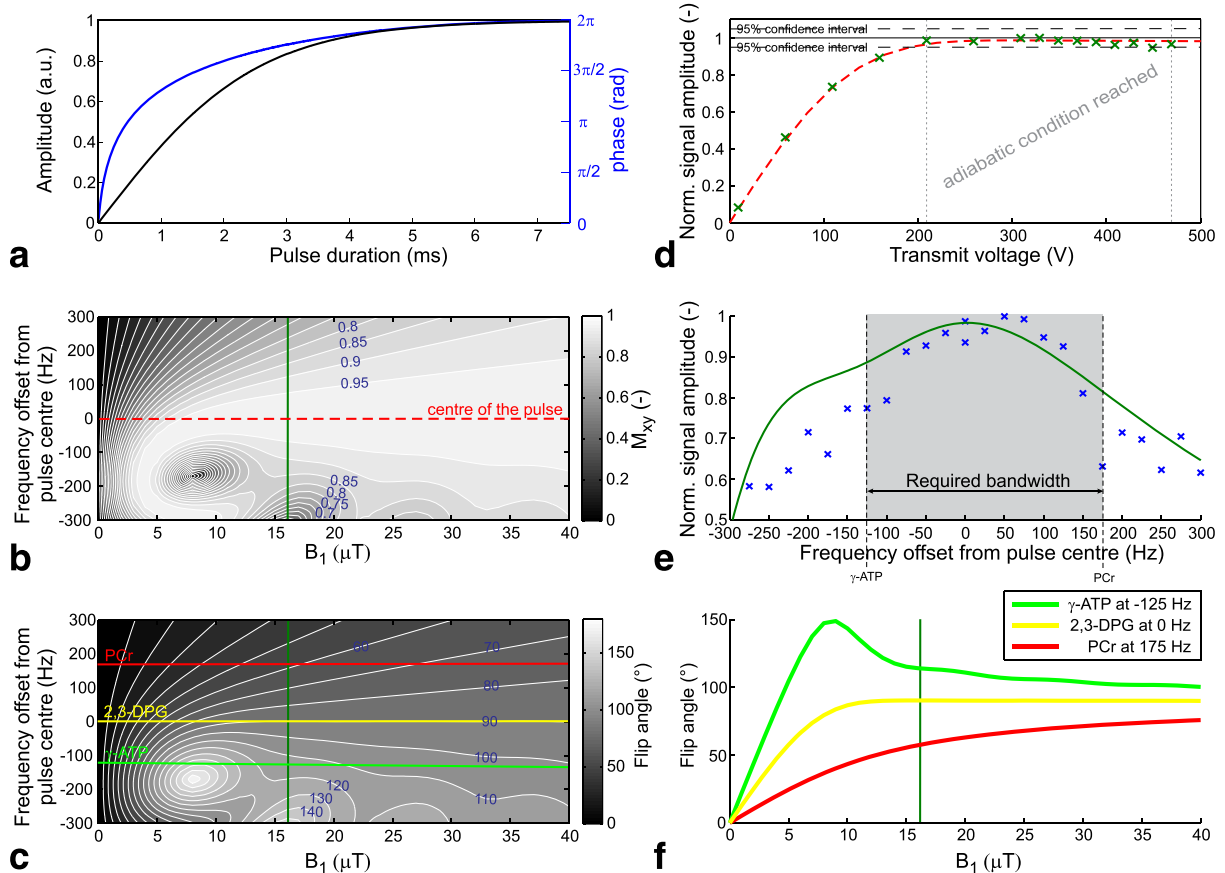
FIG. 1. Simulations of the excitation pulse with embedded results from phantom experiments. (**a**) Amplitude and phase of the adjusted 7.5-ms-long tanh/tan AHP excitation pulse. (**b**) Bloch simulation of the amount of magnetization flipped to the xy plane after the AHP excitation pulse, the center of which (0 Hz) is shifted relative to PCr resonance frequency by -175 Hz in our in vivo experiments. The lower-limit B_1^+ value expected for the used quadrature-pair RF coil at the maximum voltage at the depth of the heart (i.e. 16 μT) is highlighted with a green line. (**c**) Simulated flip angles produced by the AHP pulse centered in vivo -175 Hz relative to PCr. The three lines represent the off-resonance positions of the metabolites of interest: green, γ-ATP (-125 Hz); red, PCr (175 Hz) as compared with the yellow on-resonance behavior expected for 2,3-DPG during second acquisition. (**d**) Simulated dependence of the M_{xy} on the transmit voltage applied to the RF coil used, overlaid with the normalized signal amplitudes acquired in the localization phantom (green ×) at the depth of the heart. A 95% confidence interval delimits the plateau region where the amplitude is stable, indicating adiabatic 90° excitation. (**e**) Profile of the pulse simulated for a B_1^+ of 16 μT (green line) and as measured in the two-compartment phantom at the depth of the heart (blue ×). The BW required to excite both PCr and γ-ATP (i.e. ~300 Hz at 7 T) is also depicted. Note that the BW is shifted from the center, ranging from -125 Hz (γ-ATP) to 175 Hz (PCr), because of the asymmetry of the AHP pulse. (**f**) Flip angle as a function of B_1^+. Note the high stability of the flip angles for each metabolite (COV equal to 0.1, 2.7, and 5.6% for 0 Hz (2,3-DPG), -125 Hz (γ-ATP) and 175 Hz (PCr) excitation offset, respectively) for B_1^+ values expected in the heart (16–25 μT). This influences the saturation correction factors for γ-ATP and PCr by less than 2.5 and 2.8%, respectively, given the ranges of flip angles, metabolite T_1s, and the used TR.

therefore 6000 ms). Thus, to retain the acquisition time below 50 min, and to keep skeletal muscle contamination to a minimum, the spatial resolution in sagittal direction was sacrificed, yielding a matrix size of $8 \times 16 \times 8$ (16 in the anterior–posterior direction) over a field of view of $240 \times 240 \times 200$ mm^3, using weighted acquisition with five averages in the center of k-space. The acquisition BW of 6000 Hz was sampled by 1024 points. The resulting measurement time was 46 min and 42 s for each of the two UTE-CSI acquisitions.

Data Analysis

The amplitudes of the acquired phantom data were evaluated in MATLAB and compared to confirm the minimum transmit voltage giving 90° excitation on-resonance at the depth of the heart. Similarly, the simulated excitation profile of the AHP pulse was validated using the amplitudes of the off-resonance phantom measurements.

For each subject, three septal voxels in the two mid-SA slices (six in total) were selected for further analysis (Fig. 2b). Spectra from these voxels were phased to fix the first-order phase, and fitted using a MATLAB implementation of the time-domain fitting routine AMARES [31]. The PCr and γ-ATP signals, quantified from the first data set, were corrected for differences in T_1 relaxation using the simulated off-resonance FAs (Fig. 1f) and applying literature T_1 values for cardiac ^{31}P-MRS at 7 T [4]. The same correction factors were used for both UTE-CSI experiments with different transmit voltages. The 2,3-DPG signals were taken from the second data set and used to correct the calculated PCr/ATP ratio for blood contamination by subtracting 15% of the total 2,3-DPG signal from the γ-ATP signal [29].
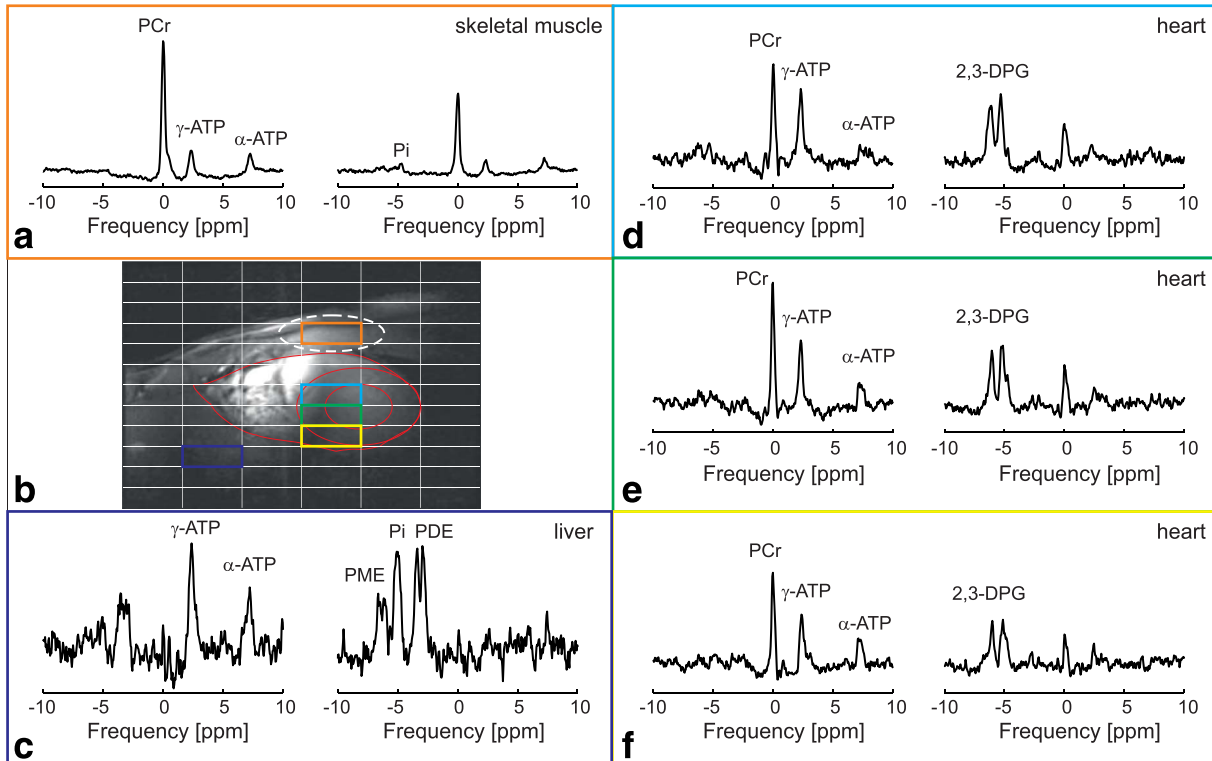
FIG. 2. Typical acquired spectra from skeletal muscle (**a**), liver (**c**), and from three of the selected voxels from the heart septum (**d–f**). (**b**) Short-axis 7T CINE FLASH localizer image showing the position of the selected voxels whose spectrum is plotted in the other panels. In panels showing ^{31}P-MR spectra, the spectra acquired with the excitation pulse centered at -175 Hz between PCr and γ-ATP are depicted on the left, whereas spectra acquired with the excitation pulse centered at 700 Hz between the 2,3-DPG resonance lines are depicted on the right. The heart is outlined in red. The simulated voxel size, affected by weighted acquisition, is depicted using a dashed white line.

To compare the two acquisitions with different transmit voltages and to demonstrate that the adiabatic onset has been reached in vivo at the lower voltage, Bland-Altman analyses of agreement (32) were performed on the blood-corrected PCr/ATP ratios; first for all 54 evaluated voxels and then for the mean PCr/ATP ratios from each of the nine volunteers. A two-way random intraclass coefficient (ICC[2,2]) of absolute agreement (33) was evaluated for the mean blood-corrected PCr/ATP ratios using SPSS (IBM SPSS, Chicago, IL) as a measure of reliability of the repeated measurement.

RESULTS

The dependence of signal amplitudes of KH_2PO_4(aq), acquired in the phantom simulating the position of the myocardium, on the applied transmit voltage is depicted together with the theoretical values in Figure 1d. The amplitude increases steadily and then plateaus from 210 V upward. The off-resonance performance of the AHP pulse as measured in the phantom is depicted in Figure 1e together with the BW predicted for comparable B_1^+.

Figure 2 depicts typical in vivo spectra acquired in skeletal muscle, liver, and in three of the selected voxels of the heart septum. Low contamination of the septal voxels by signal from the chest muscles is demonstrated. Because of the limited BW of the AHP pulse, the first interleaved spectra (left in each pair) contain only PCr, γ-ATP signals, and a minor α-ATP signal, whereas the

second interleaved spectra (right in each pair) provide the 2,3-DPG signals. Based on the Bloch simulations performed using the T_1 of PCr at 7 T (4), the experimental TR and the expected B_1^+ in the myocardium, the M_{xy} of PCr after interleaved excitation is by less than 5% lower
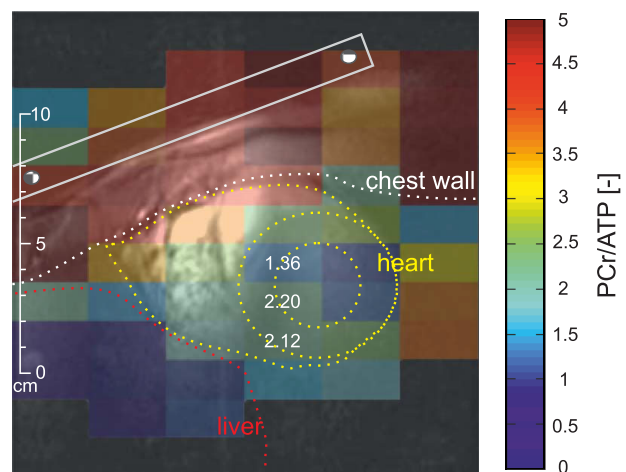

FIG. 3. Typical PCr/ATP map, after blood correction, from the same volunteer depicted in Figure 2. The map shows reasonable consistency across the midsection of the LV (mean COV less than 27%). Chest muscles exhibit much higher PCr/ATP ratio (average 4.64 ± 1.10), and the liver tissue shows negligible PCr/ATP (average 0.51 ± 0.31).

Table 1
Mean Blood-Corrected PCr/ATP Ratios of Each Volunteer Measured by Interleaved UTE-CSI Sequence Using Two Different Transmit Voltages

| Subject | PCr/ATP | | |
	MaxV	MaxV-50V	Mean
1	1.96 ± 0.29	1.94 ± 0.43	1.95 ± 0.35
2	2.01 ± 0.37	1.85 ± 0.47	1.93 ± 0.38
3	1.93 ± 0.37	2.08 ± 0.38	2.00 ± 0.30
4	2.27 ± 0.28	2.23 ± 0.58	2.25 ± 0.39
5	2.14 ± 0.52	2.13 ± 0.64	2.13 ± 0.55
6	2.02 ± 0.45	2.20 ± 0.55	2.11 ± 0.47
7	2.19 ± 0.27	2.11 ± 0.35	2.15 ± 0.27
8	2.47 ± 0.59	2.38 ± 0.66	2.42 ± 0.61
9	2.22 ± 0.29	2.33 ± 0.31	2.28 ± 0.29
Mean	**2.13 ± 0.17**	**2.14 ± 0.17**	**2.14 ± 0.16**

Note: Values are given as the mean (± SD) of the six selected voxels of the heart for each individual subject and as the mean (± SD) of the volunteers for the mean value. The intrasubject SDs are influenced by partial overlapping of the neighboring voxels.

than the M_{xy} for a single excitation with a 6-s TR. Details of this calculation are provided in the Appendix in the Supporting Information.

Figure 3 depicts a typical PCr/ATP map that is corrected for blood signal. A relatively consistent ratio across the whole left ventricle (LV) can be noticed. The mean intervoxel coefficient of variation (COV) through the LV beyond the selected voxels was 26.6 ± 3.9%. The mean PCr/ATP ratio calculated from the selected voxels was 2.13 ± 0.17 and 2.14 ± 0.17 for first and second UTE-CSI acquisitions, respectively. The mean blood-corrected PCr/ATP ratios determined for every volunteer from each UTE-CSI acquisition are given in Table 1. Considerably higher values are present in the skeletal muscles of the chest wall (4.64 ± 1.10), whereas the liver region expresses minor PCr/ATP ratios (0.51 ± 0.31). The effective size of the ellipsoidal voxel (34) resulting from weighted

acquisition, calculated at 64% of the main lobe (35) of the simulated point-spread function, was 50.7 mL. Comparing the two UTE-CSI acquisitions by the Bland-Altman plots (Fig. 4), a mean bias of −0.005 could be identified for both cases (i.e. individual voxels and volunteer means). The ICC(2,2) of the absolute agreement between the results of the two UTE-CSI acquisitions was 0.883.

DISCUSSION

In our study, we propose an interleaved UTE-CSI sequence with adiabatic excitation at 7 T to measure PCr/ATP in the human heart. This approach allows adiabatic excitation, which makes the calculation of the blood-corrected PCr/ATP throughout the sensitive volume of the coil more robust. The feasibility of the adiabatic excitation was investigated in phantom experiments and also in vivo in a group of healthy volunteers. High repeatability of the PCr/ATP measurement at 7 T was achieved with our technique, even though reduced transmit voltage was used in the second experiment.

In our localization phantom experiments, an increase in transmit voltage led, at first, to a steady increase in the acquired signal amplitude, which then plateaued. This indicated that an adiabatic threshold was reached and a B_1^+-insensitive excitation was achieved with our AHP pulse at the depth of the heart at 210 V and above. Good agreement was found between the phantom results and the Bloch simulations. Similarly, the measured excitation profile of the AHP pulse agreed well with the simulated results. Although the BW of the AHP pulse is too narrow to excite the whole ^{31}P-MR spectrum at 7 T, for the B_1^+ values provided by our quadrature-pair RF coil (i.e. over 16 μT at the depth of the heart), it does excite effectively over a bandwidth of 300 Hz, which is sufficient to excite both PCr and γ-ATP. The excitation BW of our AHP pulse could be increased using frequency sweep cycling (FSC) as used by El-Sharkawy et al. at 3 T
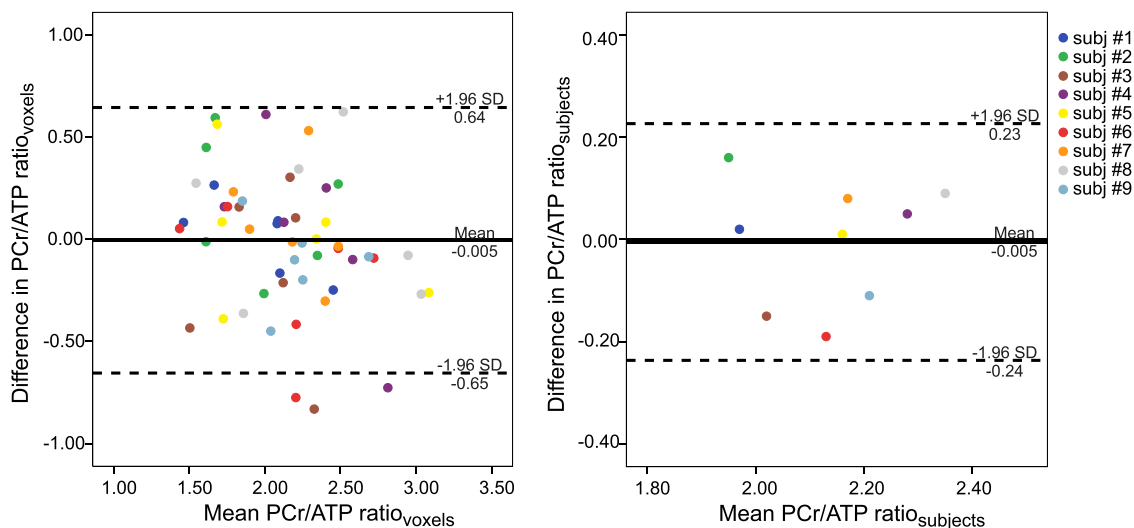
FIG. 4. Bland-Altman plots of the in vivo comparison between the scan acquired with maximum voltage applied and with 50 V less for the PCr/ATP ratio. Figure on the left depicts the comparison for all 54 selected voxels, and figure on the right shows the comparison for the volunteer means. The mean difference between the two scans is −0.005, showing only minimal bias. The repeatability coefficients are 0.65 and 0.23 for the voxel-wise and volunteer-wise analyses, respectively.

(26). However, FSC requires paired acquisition for each phase-encoding step of the CSI matrix, and therefore would significantly prolong the measurement time unless combined with a sparse k-space sampling and non-Fourier reconstruction.

To acquire the 2,3-DPG signal, which is necessary for correction on the blood ATP signal, two consecutive CSI scans, first for PCr and γ-ATP, and second for 2,3-DPG, could be performed. However, we chose to implement an interleaved excitation scheme instead. Exciting PCr and γ-ATP signals during odd transients and 2,3-DPG in the even transients effectively means that the acquisition of the second data set is shifted in time by only one TR. This allows for quantification of all metabolites of interest under the same physiological conditions. Additionally, it also means that the interleaved approach effectively doubles the TR experienced by each metabolite, decreasing the influence of any uncertainties in the T_1 used for saturation correction. This is of particular importance in patient studies as the pathology may alter the T_1 values, as shown in the liver (36). If a simple, not interleaved, excitation experiment was performed using the effective TR of 6 s, the use of a more SAR-demanding (e.g., longer) AHP pulse would be possible; however, adiabatic excitation of all metabolites of interest simultaneously would require a bandwidth of approximately 1000 Hz, which is more than three times as much as required for the presented approach. This could not be achieved for the B_1^+ range of our coil (16–25 μT), expected in the heart, by doubling or tripling the length of the AHP pulse. In addition, the unwanted T_2 relaxation occurring during the pulse duration is inherently more pronounced in very long excitation pulses, which often makes them impractical.

Acquisition of good-quality cardiac ^{31}P-MR spectra without contamination was achieved using the proposed approach. This was true also in segments of the LV beyond the septal voxels selected previously for further analysis, as the blood-corrected PCr/ATP ratio was found to be reasonably consistent across the LV (mean COV less than 27%). Although the B_1^+ of the used RF coil unfortunately did not allow acquisition of ^{31}P-MR spectra from the whole heart, it was possible to cover the whole intraventricular septum and between one-half and two-thirds of the LV, depending on the individual heart orientation. In contrast to the myocardium, the chest muscles exhibited a higher PCr/ATP ratio, and the liver tissue showed negligible PCr/ATP ratios. This is encouraging, because there is no PCr present in healthy human liver. Consistent blood-corrected PCr/ATP ratios across the heart provide further evidence of homogeneous excitation flip angle throughout the sensitive volume of the RF coil used. Looking at the actual blood-corrected PCr/ATP in the heart, all calculated ratios for each volunteer, from both acquisitions as well as the mean value of 2.14 ± 0.16, fall inside the range of literature values in healthy volunteers (4,10,37–39).

Directly comparing the results of the two UTE-CSI acquisitions for all 54 evaluated voxels by a Bland-Altman analysis of agreement, a mean bias between the measurements of -0.005 and a repeatability coefficient of 0.65 could be identified. Furthermore, by comparing the mean PCr/ATP ratios of each volunteer between

acquisitions (i.e. nine repeated measurements), the repeatability coefficient improved to 0.23. This represents higher repeatability than the previously reported interscan repeatability at 3 T, in which the PCr/ATP, averaged over three septal voxels, was measured in 20 healthy volunteers (39). In the aforementioned study, Tyler et al. (39) reported a mean interscan bias of -0.07 with a repeatability coefficient of 1.1. However, a larger nominal voxel size was used here (11.3 mL versus 5.6 mL in (39)), and both acquisitions were performed within the same session. Nevertheless, this result supports our phantom data and indicates that we have exceeded the adiabatic onset in the heart in vivo.

A limitation of our method is the overall measurement time, caused by the relatively long TR (3 s) that is necessary to comply with the legal SAR limits, and because of the need to interleave the 2,3-DPG acquisitions. Still, 3D-CSI acquisition was possible in less than 47 min. Furthermore, the measurement time could be potentially reduced through shortening of the TR, as our results suggest that a lower transmit voltage would suffice for adiabatic excitation. Alternatively, faster localization strategies (e.g., one-dimensional (1D) image selected in vivo spectroscopy (1D-ISIS)) could be combined with the adiabatic excitation and interleaved acquisition scheme presented here. However, the volume selected by 1D-ISIS depends on the sensitivity of the coil in the other two spatial directions. Therefore, 1D-ISIS is more suitable for small-diameter surface receive coils, as these are automatically insensitive to potentially contaminating tissue separated from the heart in the other two spatial directions. Our transmit/receive quadrature coil design provides the necessary B_1^+ at the depth of the heart, but its sensitivity volume in receive mode is too large to permit a clear-cut selection of signal from the heart by 1D localization. Hence, we used a 3D-CSI spatial-encoding scheme in this study. Another limitation is the small residual PCr signal noticeable in the second data sets with excitation targeted at 2,3-DPG. However, as this comprises less than 5% difference in M_{xy} using the interleaving against single excitation, its influence on the PCr/ATP ratio has been neglected. No cardiac gating was used in this study to avoid the possibility of bias due to increased miss-triggering at 7 T (40). However, in future studies, acoustic cardiac gating (40) could be applied to reduce the cardiac motion influence on data quality.

In conclusion, our proof-of-concept study demonstrates that adiabatic excitation can be achieved in human heart at 7 T. We have inserted an AHP pulse with a relatively narrow BW and introduced interleaved excitation scheme into a UTE-CSI sequence, enabling acquisition of consistent blood-corrected PCr/ATP ratios. The use of a novel quadrature RF coil increased the available peak B_1^+, thus supporting the feasibility of adiabatic excitation at 7 T. This work paves the way for the first human studies with absolute quantification of cardiac ^{31}P metabolites at 7 T.

REFERENCES

1. Bottomley PA, Charles HC, Roemer PB, Flamig D, Engeseth H, Edelstein WA, Mueller OM. Human in vivo phosphate metabolite imaging with 31P NMR. Magn Reson Med 1988;7:319–336.

2. Neubauer S. Mechanisms of disease—the failing heart—an engine out of fuel. N Engl J Med 2007;356:1140–1151.

3. Lee JH, Komoroski RA, Chu WJ, Dudley JA. Methods and applications of phosphorus NMR spectroscopy in vivo. Annu Rep NMR Spectro 2012;75:115–160.

4. Rodgers CT, Clarke WT, Snyder C, Vaughan JT, Neubauer S, Robson MD. Human cardiac 31P magnetic resonance spectroscopy at 7 Tesla. Magn Reson Med 2014;72:304–315.

5. Valkovič L, Chmelík M, Ukropcová B, et al. Skeletal muscle alkaline Pi pool is decreased in overweight-to-obese sedentary subjects and relates to mitochondrial capacity and phosphodiester content. Sci Rep 2016;6:20087.

6. Bottomley PA, NMR Spectroscopy of the human heart. In: Harris RK, Wasylishen RE, editors. Encyclopedia of Magnetic Resonance. Chichester, U.K.: John Wiley; 2009.

7. Bottomley PA, Herfkens RJ, Smith LS, Bashore TM. Altered phosphate metabolism in myocardial infarction: P-31 MR spectroscopy. Radiology 1987;165:703–707.

8. Conway MA, Allis J, Ouwerkerk R, Niioka T, Rajagopalan B, Radda GK. Detection of low phosphocreatine to ATP ratio in failing hypertrophied human myocardium by P-31 magnetic-resonance spectroscopy. Lancet 1991;338:973–976.

9. Deroos A, Doornbos J, Luyten PR, Oosterwaal LJMP, Vanderwall EE, Denhollander JA. Cardiac metabolism in patients with dilated and hypertrophic cardiomyopathy—assessment with proton-decoupled P-31 MR spectroscopy. J Magn Reson Imaging 1992;2:711–719.

10. Neubauer S, Krahe T, Schindler R, et al. 31P magnetic resonance spectroscopy in dilated cardiomyopathy and coronary artery disease. Altered cardiac high-energy phosphate metabolism in heart failure. Circulation 1992;86:1810–1818.

11. Neubauer S, Horn M, Godde M, Harre K, Pabst T, Newell JB, Peters W, Hahn D, Ertl G, Kochsiek K. Myocardial phosphocreatine-to-ATP ratio is a predictor of mortality in patients with dilated cardiomyopathy. Circulation 1997;96:2190–2196.

12. Levelt E, Rodgers CT, Clarke WT, et al. Cardiac energetics, oxygenation, and perfusion during increased workload in patients with type 2 diabetes mellitus. Eur Heart J 2016;37:3461–3469.

13. Levelt E, Mahmod M, Piechnik SK, et al. Relationship between left ventricular structural and metabolic remodeling in type 2 diabetes. Diabetes 2016;65:44–52.

14. Rider OJ, Francis JM, Ali MK, Holloway C, Pegg T, Robson MD, Tyler D, Byrne J, Clarke K, Neubauer S. Effects of catecholamine stress on diastolic function and myocardial energetics in obesity. Circulation 2012;125:1511–1519.

15. Bogner W, Chmelik M, Schmid AI, Moser E, Trattnig S, Gruber S. Assessment of 31P relaxation times in the human calf muscle: a comparison between 3 T and 7 T in vivo. Magn Reson Med 2009;62:574–582.

16. Parasoglou P, Xia D, Chang G, Regatte RR. Dynamic three-dimensional imaging of phosphocreatine recovery kinetics in the human lower leg muscles at 3T and 7T: a preliminary study. NMR Biomed 2013;26:348–356.

17. Šedivý P, Kipfelsberger MC, Dezortová M, Krššák M, Drobný M, Chmelík M, Rydlo J, Trattnig S, Hájek M, Valkovič L. Dynamic 31P MR spectroscopy of plantar flexion: influence of ergometer design, magnetic field strength (3 and 7 T), and RF-coil design. Med Phys 2015;42:1678–1689.

18. Valkovič L, Chmelík M, Just Kukurová I, Krššák M, Gruber S, Frollo I, Trattnig S, Bogner W. Time-resolved phosphorous magnetization transfer of the human calf muscle at 3 T and 7 T: a feasibility study. Eur J Radiol 2013;82:745–751.

19. Rodgers CT, Clarke WT, Berthel D, Neubauer S, Robson MD. A 16-element receive array for human cardiac 31P MR spectroscopy at 7T. In Proceedings of the 22nd Joint Annual Meeting of ISMRM & ESMRMB, Milan, Italy, 2014. p. 2896.

20. Stoll VM, Clarke WT, Levelt E, Liu A, Myerson SG, Robson MD, Neubauer S, Rodgers CT. Phosphorus 31P magnetic resonance spectroscopy at 7 Tesla in patients with dilated cardiomyopathy. Radiology 2016;281:409–417.

21. Ouwerkerk R, Bottomley PA. On neglecting chemical exchange effects when correcting in vivo 31P MRS data for partial saturation. J Magn Reson 2001;148:425–435.

22. Chmelík M, Považan M, Jiru F, Just Kukurová I, Dezortová M, Krššák M, Bogner W, Hájek M, Trattnig S, Valkovič L. Flip-angle mapping of 31P coils by steady-state MR spectroscopic imaging. J Magn Reson Imaging 2014;40:391–397.

23. Clarke WT, Robson MD, Rodgers CT. Bloch-Siegert B1+-mapping for human cardiac 31P-MRS at 7 Tesla. Magn Reson Med 2016;76:1047–1058.

24. Rodgers CT, Robson MD. Coil combination for receive array spectroscopy: Are data-driven methods superior to methods using computed field maps? Magn Reson Med 2016;75:473–487.

25. Bottomley PA, Ouwerkerk R, Lee RF, Weiss RG. Four-angle saturation transfer (FAST) method for measuring creatine kinase reaction rates in vivo. Magn Reson Med 2002;47:850–863.

26. El-Sharkawy AM, Schar M, Ouwerkerk R, Weiss RG, Bottomley PA. Quantitative cardiac 31P spectroscopy at 3 Tesla using adiabatic pulses. Magn Reson Med 2009;61:785–795.

27. Schaller B, Paritmongkol W, Rodgers CT. Quadrature 31P and single 1H dual-tune coil for cardiac 31P-MRS at 7T. In Proceedings of the 24th Annual Meeting of ISMRM, Singapore, 2016. p. 4006.

28. Garwood M, Ke Y. Symmetrical pulses to induce arbitrary flip angles with compensation for RF inhomogeneity and resonance offsets. J Magn Reson 1991;94:511–525.

29. Horn M, Kadgien M, Schnackerz K, Neubauer S. 31P-nuclear magnetic resonance spectroscopy of blood: a species comparison. J Cardiovasc Magn Reson 2000;2:143–149.

30. Robson MD, Tyler DJ, Neubauer S. Ultrashort TE chemical shift imaging (UTE-CSI). Magn Reson Med 2005;53:267–274.

31. Purvis LAB, Clarke WT, Biasiolli L, Robson MD, Rodgers CT. Linewidth constraints in Matlab AMARES using per-metabolite T2 and per-voxel ΔB0. In Proceedings of the 22nd Joint Annual Meeting of ISMRM & ESMRMB, Milan, Italy, 2014. p. 2885.

32. Altman DG, Bland JM. Measurement in medicine—the analysis of method comparison studies. Statistician. 1983;32:307–317.

33. Shrout PE, Fleiss JL. Intraclass correlations: uses in assessing rater reliability. Psychol Bull 1979;86:420–428.

34. Scheenen TW, Klomp DW, Roll SA, Futterer JJ, Barentsz JO, Heerschap A. Fast acquisition-weighted three-dimensional proton MR spectroscopic imaging of the human prostate. Magn Reson Med 2004;52:80–88.

35. Pohmann R, von Kienlin M. Accurate phosphorus metabolite images of the human heart by 3D acquisition-weighted CSI. Magn Reson Med 2001;45:817–826.

36. Cox IJ, Coutts GA, Gadian DG, Ghosh P, Sargentoni J, Young IR. Saturation effects in phosphorus-31 magnetic resonance spectra of the human liver. Magn Reson Med 1991;17:53–61.

37. Hardy CJ, Weiss RG, Bottomley PA, Gerstenblith G. Altered myocardial high-energy phosphate metabolites in patients with dilated cardiomyopathy. Am Heart J 1991;122:795–801.

38. Meininger M, Landschutz W, Beer M, et al. Concentrations of human cardiac phosphorus metabolites determined by SLOOP 31P NMR spectroscopy. Magn Reson Med 1999;41:657–663.

39. Tyler DJ, Emmanuel Y, Cochlin LE, Hudsmith LE, Holloway CJ, Neubauer S, Clarke K, Robson MD. Reproducibility of 31P cardiac magnetic resonance spectroscopy at 3 T. NMR Biomed 2009;22:405–413.

40. Frauenrath T, Hezel F, Renz W, et al. Acoustic cardiac triggering: a practical solution for synchronization and gating of cardiovascular magnetic resonance at 7 Tesla. J Cardiovasc Magn Reson 2010;12:67.

SUPPORTING INFORMATION

Additional Supporting Information may be found in the online version of this article.

Fig. S1. Simulations of the M_{xy} under (**a**) ideal and (**b**) real steady-state conditions for a given experimental TR and metabolite T_1, as defined previously. (**c**) Simulated dependences of the Mxy on the B_1^+ for the resonance offset of PCr (175 Hz). The ideal steady-state M_{xy} dependence is represented by a black line; the real steady-state condition is represented by a blue line (full = odd and dashed = even transient). (**d**) Ratio of PCr M_{xy} excited during even and odd transients (green) and the percentage difference between the ideal and real (odd) M_{xy} of PCr (red).

Appendix. Quantification of the Influence of Partial PCr Excitation Using Interleaved Approach